Development of the Deployable on-Orbit ultraLight Composite Experiment (DOLCE) for the Space Solar Power Project (SSPP) Demonstration Mission

Eleftherios E. Gdoutos,* Charles F. Sommer,† Alan Truong,‡ Alexander Wen,§ Antonio Pedivellano,¶ Uba K Ubamanyu,‖ Richard G. Madonna,** and Sergio Pellegrino††
California Institute of Technology, Pasadena, CA, 91125

We describe the development of an engineering model of the DOLCE payload which will demonstrate on orbit for the first time the deployment of an ultralight Caltech SSPP structure. Deployment tests at the subsystem and system levels, launch load analysis and testing, and accelerated aging tests have been conducted. The DOLCE payload will be launched with the SSPD-1 mission which will demonstrate space-based solar power key enabling technologies in photovoltaics, power beaming, and deployable structures.

I. Introduction

Large spacecraft collecting solar power and wirelessly transmitting it to Earth were first proposed in 1968 [1]. Since then, multiple concepts to implement space-based solar power have been described, but none have been realized [2–7]. Recent technology developments are progressively increasing the capability toward the realization of space-based solar power [8]. In 2016, the Caltech SSPP team identified key research areas required to enable the viability of space-based solar power and formulated a concept based on advances in these research areas [9].

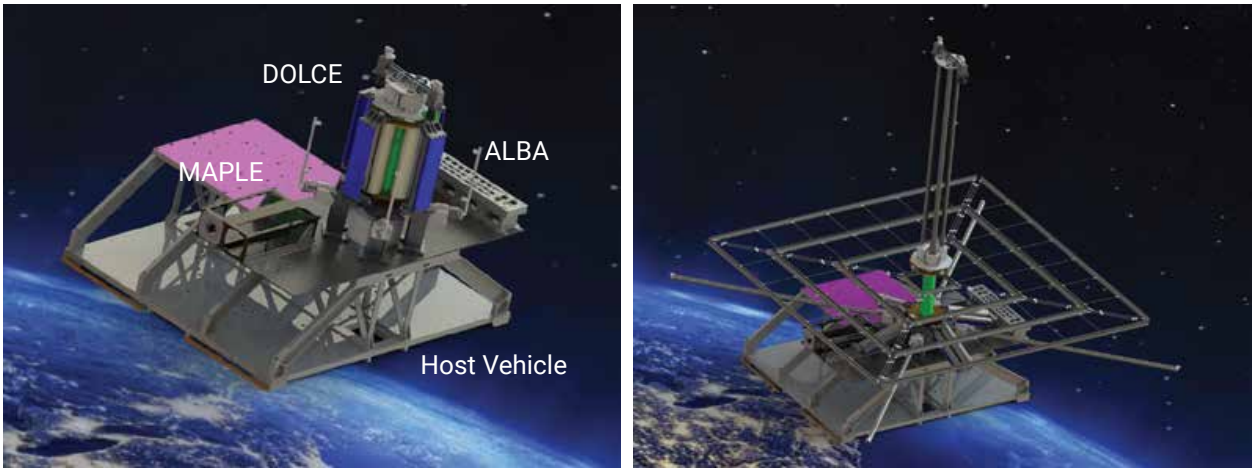

(a) (b)

Fig. 1 SSPD-1 rendering on host spacecraft (a) prior to and (b) after DOLCE deployment.

Between 2017 and 2019, the Caltech team demonstrated two lab prototypes of the lightest to-date multi-functional units that integrate solar power collection and steerable wireless power transfer [10–12]. In 2019 and 2020, the Caltech

*Principal Research Scientist, Graduate Aerospace Laboratories, MC 105-50, Pasadena. AIAA Member. E-mail: egdoutos@caltech.edu.
†Research Engineer, Graduate Aerospace Laboratories, MC 105-50, Pasadena.
‡Research Engineer, Graduate Aerospace Laboratories, MC 105-50, Pasadena.
§PhD Candidate, Graduate Aerospace Laboratories, MC 105-50, Pasadena. AIAA Student Member.
¶PhD Graduate, Graduate Aerospace Laboratories, MC 105-50, Pasadena. Currently at DCubeD GmbH, Burgweg 6, 82110 Germering, Germany.
‖PhD Candidate, Graduate Aerospace Laboratories, MC 105-50, Pasadena. AIAA Student Member.
**Project Manager, Caltech Space Solar Power Project; Proprietor, Systems Engineering Consultants, Columbia, Md.
††Joyce and Kent Kresa Professor of Aerospace and Civil Engineering; Jet Propulsion Laboratory Senior Research Scientist; Co-Director, Space-Based Solar Power Project, Graduate Aerospace Laboratories, MC 105-50. AIAA Fellow. E-mail: sergiop@caltech.edu.

team demonstrated the first packageable and deployable lab prototypes of ultralight (150 g/m^2), bending-stiff thin-shell space structures (Caltech SSPP structures) scalable to 60×60 m^2 and designed for integration with multi-functional elements. This large ultralight deployable is one of the key enabling technologies for space-based solar power and missions requiring large ultralight solar arrays and phased-array antennas [13–15].

The Space Solar Power Demonstration-1 (SSPD-1) mission (target launch Q4 2022) was established to advance the readiness level, investigate the on-orbit performance, and demonstrate, for the first time on orbit, the space-based solar power technologies researched at Caltech since 2016. SSPD-1 is a 45 kg, 80 W LEO mission consisting of three payloads: DOLCE, ALBA, and MAPLE. DOLCE is a deployment demonstration of Caltech's SSPP structure. ALBA will evaluate the performance and future mission suitability of emerging photovoltaic materials. MAPLE is a wireless power transfer demonstration using Caltech's unique flexible PCB phased array design to beam power over a short distance to an array of receiving antennas.

Here, we present a brief overview of the SSPD-1 and DOLCE mission. We describe the DOLCE deployable structure and deployment mechanism design, and present results and lessons learned from DOLCE's functional and launch load testing.

II. SSPD-1 and DOLCE Mission Overview

SSPD-1, shown in CAD-render in Figure 1a, will be hosted on a Momentus Vigoride spacecraft launched to a 550 km sun synchronous orbit as an ESPA payload on a Falcon 9. SSPD-1 remains attached to the host spacecraft that provides power, orbit and attitude keeping, and communication to the ground. DOLCE, MAPLE, and ALBA are each built and operated as separate, individual payloads. The main limitations for concurrent operation are power availability and the DOLCE deployable structure shading the ALBA PV after deployment. The arrangement of the different payloads on the host vehicle minimizes the overall volume, while ensuring no interference with the deployment of DOLCE's structure. A central avionics system communicates between the host spacecraft and each payload, controls which payload is active, and distributes power from the host spacecraft to each payload as needed for each payload's individual experiments. The avionics system uses a Xiphos Q7s on-board computer with the MAX flight-software developed by ASI (RocketLab) and a GOMSpace Nanopower P60 power supply.

DOLCE is a technology demonstration mission with two objectives: to demonstrate the on-orbit deployment of a prototype-scale (1.7 m $\times$ 1.7 m) Caltech SSPP structure and to characterize the response of the deployed structure under space environment disturbances.

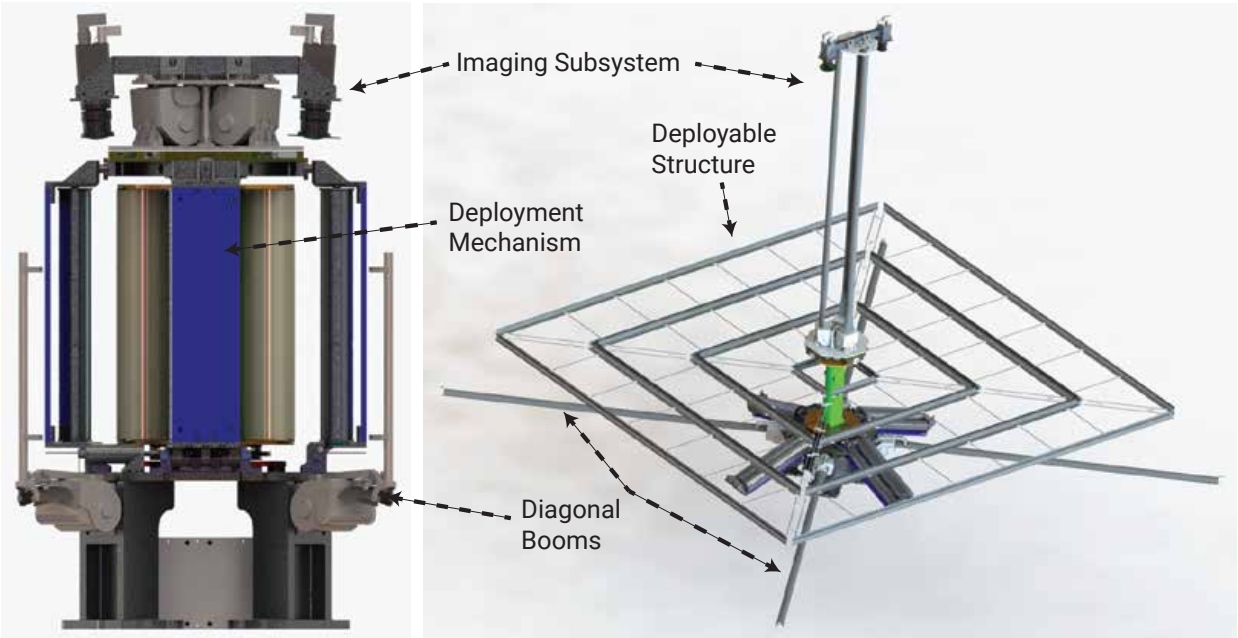

Fig. 2 DOLCE in stowed (left) and deployed (right) configurations

The DOLCE deployment sequence of operations and power consumption are listed in Table 1. The sequence of operations concludes with the deployment of the Caltech SSPP structure, which is captured in video by cameras deployed on a boom perpendicular to the plane of the structure, as shown in Figure 1b. After completion of the deployment sequence images of the deployed structure will be captured and analyzed to determine the structure's response to space environment disturbances.

Four subsystems comprise the DOLCE payload (Figure 2): (1) Deployable Structure; (2) Deployment Mechanism; (3) Diagonal Booms; and (4) Imaging Subsystem. The DOLCE volume envelope is 500 mm (l) × 500 mm (w) × 750 mm (h) and the nominal and current best estimate (CBE) mass breakdowns are shown in Table 2.

Table 1 DOLCE deployment operations sequence and power usage

Operation	Approximate Duration	Average / Peak Power (W)
Deploy camera boom	15 minutes	58 / 78
Deploy four diagonal booms sequentially	40 minutes	41 / 52
Uncoil structure	30 seconds	57 / 67
Extend four diagonal booms sequentially	20 minutes	41 / 52
Deploy structure	< 1 second	31 / 81

Table 2 DOLCE Nominal and CBE mass

Subsystem	Nominal Mass (kg)	Contingency	CBE mass (kg)
Deployable Structure	0.29	1.07	0.31
Deployment Mechanism	23.84	1.08	25.70
Diagonal Booms and Controller	4.43	1.08	4.78
Imaging Subsystem	3.04	1.12	3.39
Total	**31.60**	**1.08**	**34.18**

III. DOLCE Design

The novel technologies that DOLCE aims to demonstrate are the Caltech SSPP structure [16] and the pressure-wrapping concept [17] mechanism to deploy this structure. Therefore, the structure and mechanism were designed, built, and tested by Caltech, whereas the diagonal booms and imaging subsystem components were procured externally. Specifically, the diagonal booms and boom module that deploys the cameras were procured from MMA Design, LLC; the cameras and lenses are Imperx C2410 5 MP and Schneider Cinegon 1.8/4.8 mm, respectively, with space environment modifications made by the suppliers.

A. Deployable Structure Design

The design of the DOLCE engineering model (EM) Caltech SSPP structure evolved from previous prototype iterations. The behavior of previously fabricated Caltech SSPP structure prototypes [15] was characterized through multiple deployment tests and three key risks were identified. Table 3 lists the key risks identified and the associated mitigation redesign for the EM deployable structure.

The DOLCE EM deployable structure design is shown in Figure 3a and the assembled structure is shown in Figure 3b. The structure weighs 291 g (99 g/m^2). The longerons are TRAC [18] cross-section [+-45PWGF/0CF/+-45PWGF] composite thin shells with 70 μm flange thickness, 12.5 mm radius of curvature and 105° subtended angle. Whereas previous designs used a 90° subtended angle [19–21], the angle was increased to 105° to provide additional stiffness and ensure complete structure deployment even under gravity. The batten geometry (shown in Figure 3a) was redesigned from the previously developed prototypes to induce a deterministic fold location during deployment and to prevent the battens from stacking and developing large thickness discontinuities during coiling.

Table 3 DOLCE Deployable Structure Key Risks Identified

Key Risk	Mitigation Strategy	Design Action
Incomplete deployment	Increase longeron stiffness	Increase longeron subtended angle to 105°
Asymmetric deployment	Deterministic fold locations	Redesign batten location
Failure due to long-term stowage	Decrease time-dependency of matrix	Use cyanate ester matrix in longerons

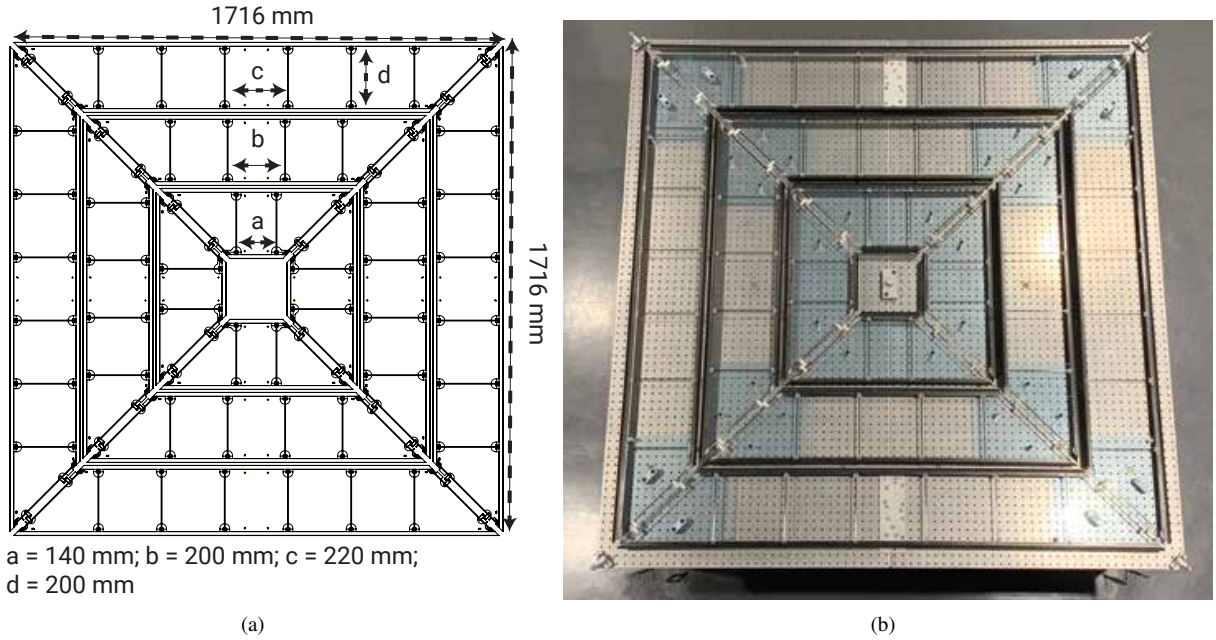

Fig. 3 DOLCE deployable structure (a) design drawing; and (b) after integration, on positioning plates (light blue)

It was previously observed that stress relaxation in the longerons in response to the imposed curvature during stowage can significantly affect the structure's deployment process and structural integrity [22–24]. To select the deployable structure matrix, which is the main contributor to time-dependent behavior in high strain composites, we compared the survivability under long-duration stowage conditions of two candidate materials: epoxy TP 402T and cyanate ester TP 380CE, both supplied by North Thin Ply Technology. The flattening to rupture (FTR) test setup described in [24] was used for this comparison.

Test coupons were manufactured with an initial curvature in the middle. These coupons consisted of plain weave glass fiber (PWGF) and uni-directional carbon fiber (UDCF) layers. The PWGF plies are 25 grams per square meter (gsm) glass fibers, while the UDCF plies are made of 30 gsm MR70 fibers. The laminate consisted of a single ±45 PWGF ply, sandwiched between two, 3-ply prepreg tape of [±45 PWGF /0 UDCF/±45 PWGF] supplied by North Thin Ply Technology. 7-ply laminates were prepared from the prepregs and cured in an autoclave using vacuum bagging with an aluminum mold that has a narrow curved region in the middle and two tangent flat regions on either side. This particular 7-ply laminate corresponds to the web-section of the EM DOLCE structure's longerons.

The curved coupons were flattened between two glass plates clamped at the edges. The relaxation process was accelerated by testing at an elevated temperature of 70 °C. The time taken for a macroscopic crack to appear was measured using a camera. The results of the test are reported in Figure 4. 40% of epoxy test samples exhibited macroscopic cracks before 10 hours at 70 °C. An additional 18% of the epoxy samples exhibited macroscopic cracks before 7 days at 70 °C, whereas only 5% of the cyanate ester samples exhibited macroscopic cracks before 7 days at 70 °C. The high survivability of cyanate ester samples indicated that, for the temperature and duration studied, a deployable structure with this laminate would be expected to exhibit insignificant loss of structural integrity due to stress relaxation. Based on the superior survivability of the cyanate ester samples, TP 380CE was selected as the matrix for the

DOLCE longerons. Further accelerated aging tests were conducted at the structure level and are described in Section IV.

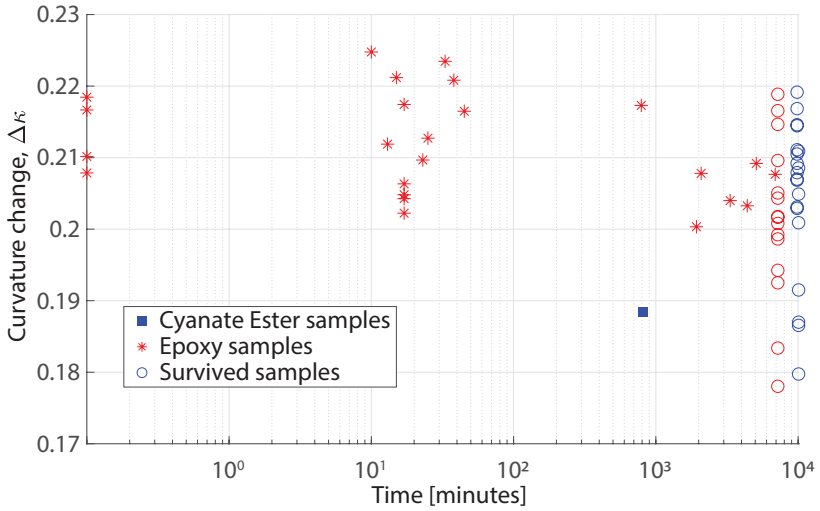

Fig. 4 Survivability comparison between epoxy and cyanate ester composite samples under imposed curvature

B. Deployment Mechanism

The DOLCE EM deployment mechanism is a design evolution of a previously described lab prototype based on the concept of pressure-wrapping [15, 17]. The deployment mechanism architecture is a center winding process that consists of a central rotation stage which drives the coiling and uncoiling operation by rotating inner cylinders. The deployable structure is coiled on the inner cylinders and four rollers that each spool a polyimide membrane provide the wrapping pressure. A schematic of the concept is shown in Figure 5.

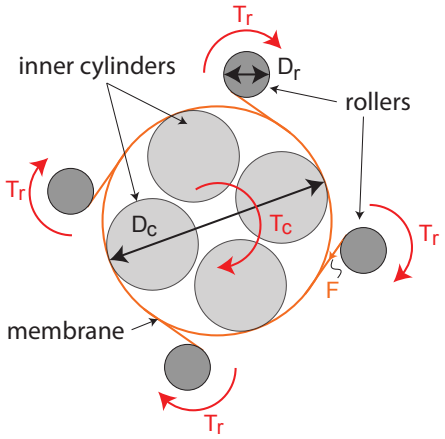

Fig. 5 Torque equilibrium of deployment mechanism. The coiled structure is held by the membrane.

The tension in the membrane F is related to the torque applied by central stage through the inner cylinders T_c and rollers T_r through the following conditions, resulting from the geometry of the mechanism:

$$T_r = F\frac{D_r}{2} \tag{1a}$$

$$T_c = 4T_r\frac{D_c}{D_r} = 2FD_c \tag{1b}$$

where $D_r = 36$ mm and $D_c = 200$ mm in the current implementation. The mechanism's CAD rendering and selected components are shown in Figure 6a and the assembled EM mechanism is shown in Figure 6b.

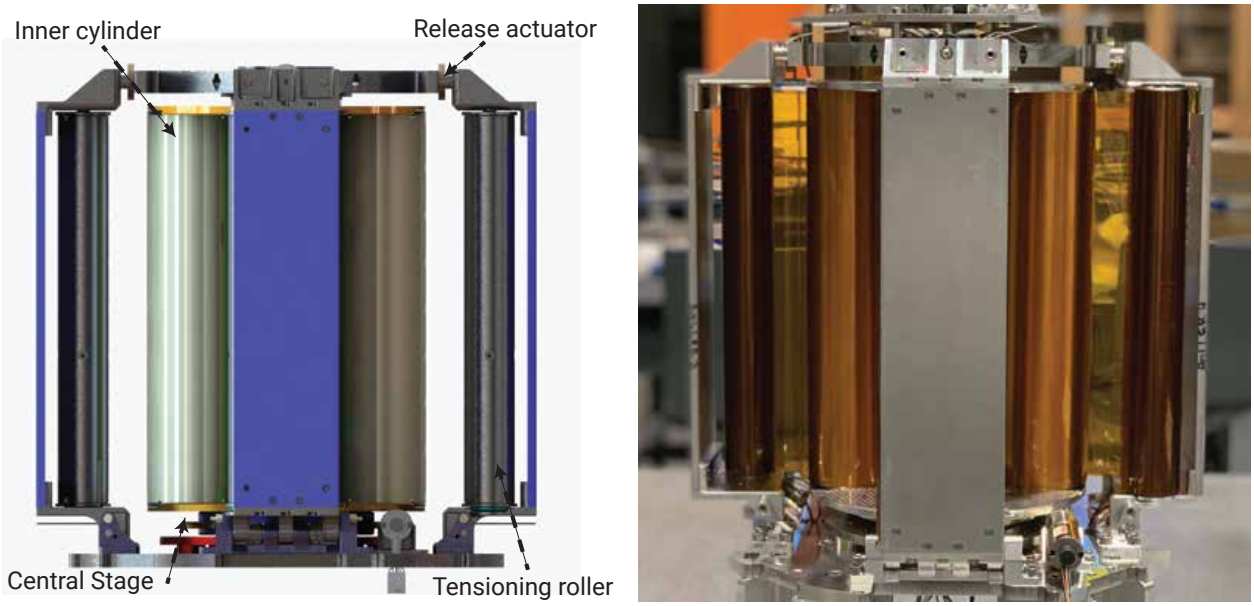

(a) (b)

Fig. 6 (a) CAD render of EM deployment mechanism; (b) assembled DOLCE EM mechanism

The implementation of the deployment mechanism requires five actuators: one to drive the rotation of the central stage and four on the membrane rollers to provide membrane tension. The selected actuators for this mission are space-rated brushed DCX22S motors equipped with the GPX22UP planetary gearhead, supplied by Maxon Precision Motors, Inc. These motors have been successfully used on the hammering mechanism of the HP^3 instrument in NASA's InSight mission [25]. The roller motors are equipped with permanent magnet detent brakes, which have been previously qualified for the Mars 2020 mission [26]. The detent brakes passively lock the roller motors, so as to maintain the tension in the membranes during launch. On the central stage side, the locking feature is provided by friction in the worm gear connecting the central motor to the central stage of the mechanism. Each motor is driven by a Maxon EPOS4 Module 24/1.5 controller, powered and controlled by the SSPD-1 avionics system.

The speed, torque, and current characteristics of the central stage and rollers are shown in Figure 7a and Figure 7b, respectively. In the plots, the currents on the x-axis refer to the output of the motor controllers and the torque values correspond to T_r and T_c in Figure 5. They are related to torque and velocity of the motors through the following relations:

$$T_r = \eta_r r_r T \tag{2a}$$

$$T_c = \eta_c r_c T \tag{2b}$$

$$n_r = \frac{n}{r_r} \tag{2c}$$

$$n_c = \frac{n}{r_c} \tag{2d}$$

where T and n are the torque and speed of the motors, r_r and r_c are the total reduction ratios on the roller and central motors, and η_r and η_c are the efficiencies of the gear train on the roller and central motor, respectively. The reduction on the rollers is provided solely by the motor planetary gearhead (r_r = 186:1 and η_r = 0.9), while the reduction on the central stage results from the contributions of the motor planetary gearhead (r_c =35:1 and η_c = 0.9) and the worm gear drive (r_{wg} =180:1 and η_{wg} = 0.15), so that the total reduction ratio and efficiency are r_c = 6300:1 and η_c = 0.135. The efficiency of the worm gear drive was measured experimentally, whereas the efficiency of the gearheads corresponds to the datasheet value.

Together, the plots in Figures 7a and 7b identify the operating conditions for the mechanism. The blue lines correspond to the upper operational limits of the motor based on voltage availability from the controller. The black dashed lines describe the maximum continuous motor operating point and the red lines correspond to the maximum

continuous output current from the motor controllers. The green shaded area indicates the operating range of the entire system, which is limited by the maximum current on the central stage motor controller, as can be observed in Figure 7a. The intersection between the red line and the blue line in this plot identifies the maximum continuous operating point for the system (maximum speed and torque), indicated by the red circle.

The shaded orange area represents the speed constraint imposed by the detent brakes on the roller motors, which is below the minimum speed necessary for smooth, continuous operation. Operating points within this region would experience significant fluctuations of the roller torque due to the periodic torque applied by the permanent magnets in the detent brakes. These effects become negligible when the speed of the roller motors before the planetary gearhead reduction is greater than 500 rpm. The nominal operating point during coiling/uncoiling (black circle in Figure 7) was therefore chosen to provide 25 N tension on the membrane and to operate at the minimum allowable speed outside of the orange region.

Figure 7 also shows the braking torque provided by the detent brakes, and the maximum startup torque required to overcome their action. The grey and blue points correspond to the braking torque range specified by the manufacturer, representing the worst case scenario from the launch lock and motor startup perspectives. During launch, the motors rely on the brakes to hold the tension in the membrane, and the worst case scenario corresponds to the lower bound of the detent brake torque (grey circle). During operation, at motor startup, the worst case scenario is having the largest possible detent torque that the motors would have to overcome (blue circle).

At the conclusion of uncoiling, the release actuators (shown in Figure 6a) are powered and the tensioning roller assembly separates from the top of the mechanism and rotates downwardly, thus allowing the deployable structure to unfold and fully deploy. The release actuators are procured from Ensign-Bickford Aerospace & Defense.

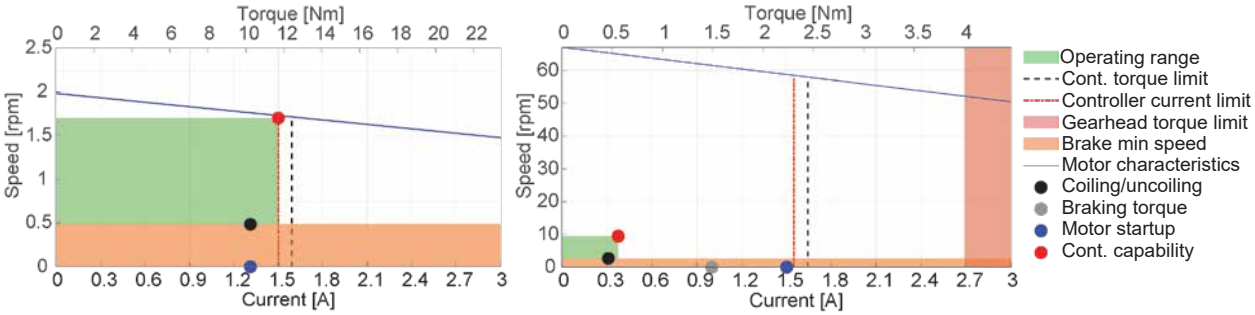

(a) Central stage characteristics

(b) Roller characteristics

Fig. 7 Deployment mechanism speed, torque, and current characteristics.

C. Structural Analysis

Structural design validation of the deployment mechanism was performed by finite element modal and loads analysis with the Abaqus software.

The model consisted of 1,291,126 linear hexahedral elements (C3D8) as shown in Figure 8 with material properties defined in Table 4. Material densities were multiplied by 1.1 to account for mass contingency. All bolted joints were modeled using tie constraints between the relevant surfaces and the hinges at the base of the tensioning rollers was modeled with connectors to accurately model the relevant degree of freedom at these locations. Increased fidelity, such as explicitly modeling discrete fasteners, was used in certain locations of interest. Other joints and more complex components, for example the bearings, were modeled as homogenized solids with stiffness tuned to match experimental results in component and subassembly level sine sweeps.

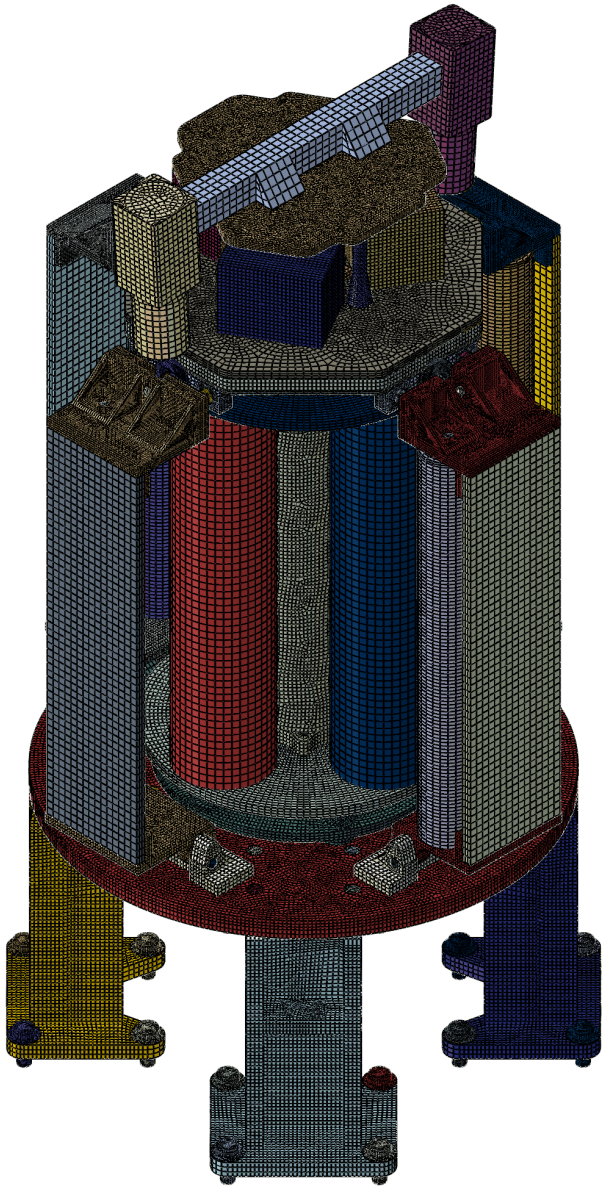

Fig. 8 Meshed FEA model of the SSPD-1 mission.

Table 4 FEA model material properties

Material	Modulus (MPa)	Poisson Ratio	Density (kg/m^3)	Yield Strength (MPa)
Aluminum	68,900	0.33	2,981	276
Bronze	117,000	0.34	9,251	172
Stainless Steel	193,000	0.29	8,800	290 / 896 (A286)
Titanium	105,000	0.31	4,873	828

The analyses performed were a linear frequency analysis (Lanczos solver) to determine the fundamental frequency of the mechanism and a linear static stress analysis (Full Newton solver) to evaluate the survivability against the quasi-static design load factor of 15 g in each direction. The modal analysis predicted that the fundamental mode corresponded to a

global bending mode at 77 Hz. Von Mises stresses were extracted from the stress analysis and margins against yield were calculated with a safety factor of 1.2 using the equation:

$$Margin = \frac{\sigma_y}{\sigma_{mises,FEA} * FoS} - 1 \tag{3}$$

The lowest margins are listed in Table 5 and their corresponding locations in the design are shown in Figure 9.

Table 5 FEA lowest margin locations

Location	Description	Margin
a	Payload mounting bolts	0.3
b	Mechanism plate mounting bolts	1.22
c	Metrology support post bolts	0.13
d	Metrology support post base threads	0.05

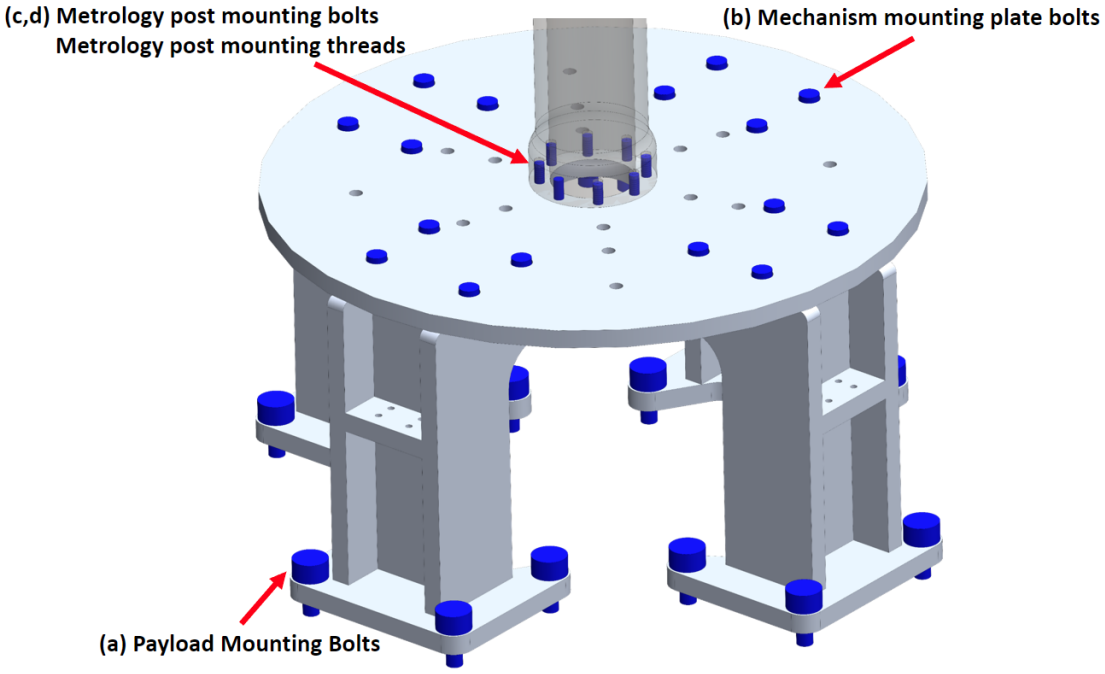

Fig. 9 Locations of lowest predicted margins.

D. Deployment Tests

Deployment tests were performed in the Caltech CAST motion capture laboratory in Pasadena to verify that the previously identified risks in structure deployment were adequately addressed and to validate the deployment mechanism design. The setup consisted of the deployable structure packaged in the deployment mechanism and the associated electronics to drive the system (Figure 10a). Aluminum frames oriented along the diagonals of the structure acted as surrogates of the deployable diagonal booms, which were not included in this setup (Figure 10b).

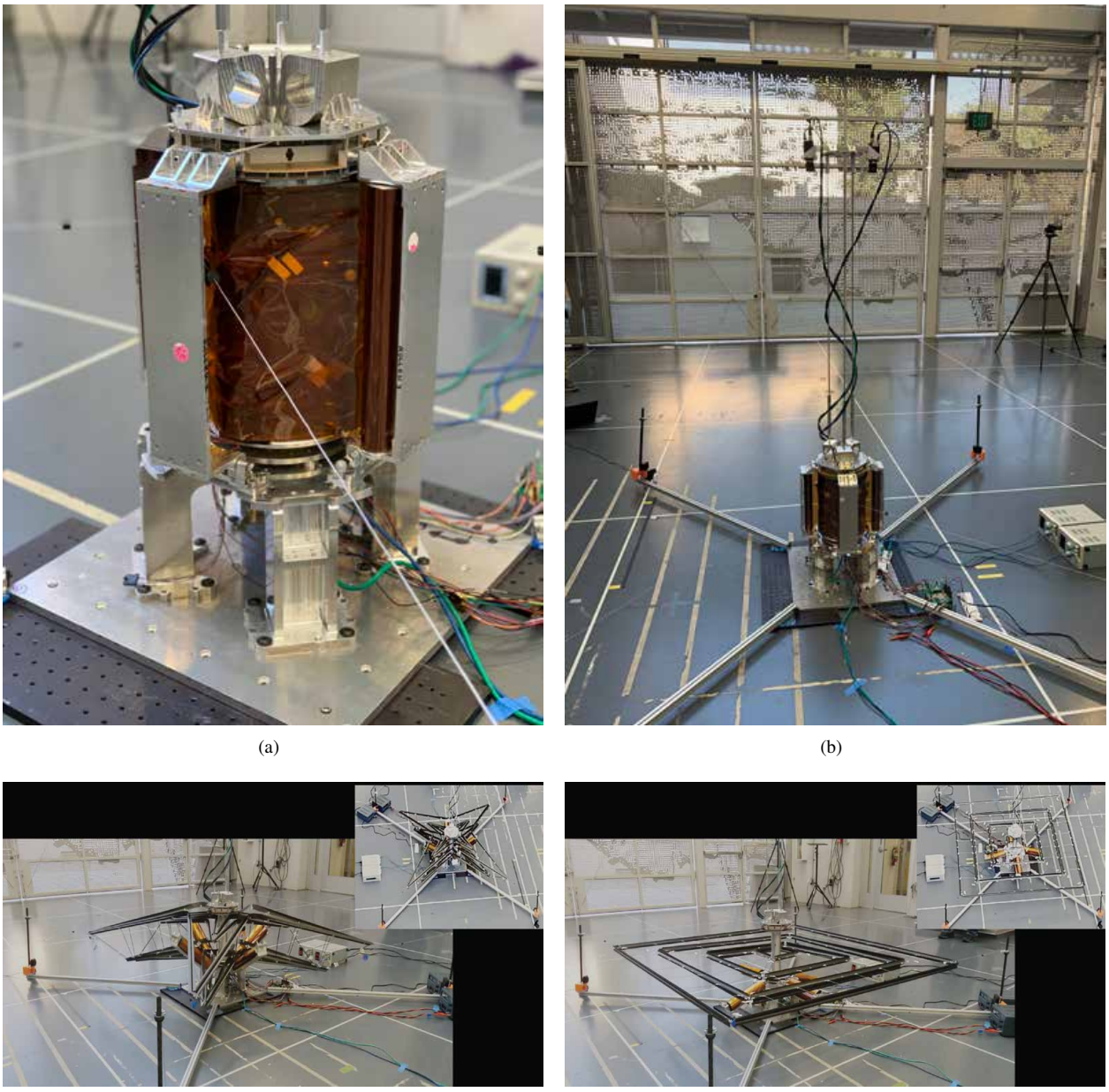

(a) (b)

(c) (d)

Fig. 10 (a) Close-up of EM deployment mechanism with structure fully packaged; (b) Overview of deployment test setup with aluminum frame boom surrogates (c) deployment mechanism releasing tensioning roller assemblies and structure during deployment; (d) structure fully deployed.

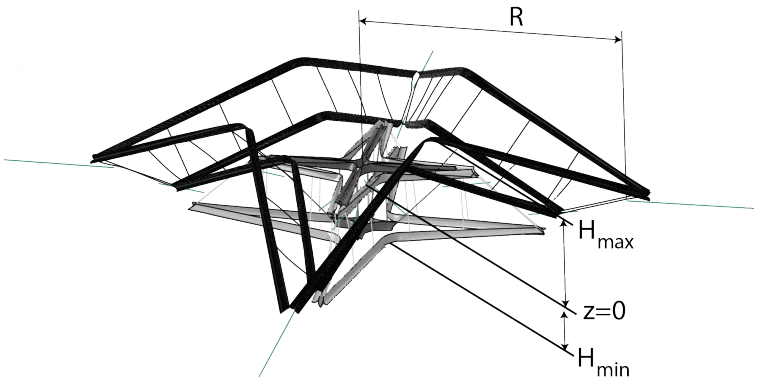

Fig. 11 Definition of metrics for deployment tests.

Measurements from the deployment tests were obtained by tracking 278 targets distributed on the structure. Their 3D coordinates were captured by an OptiTrack motion capture system (consisting of 7 Prime^X 41 cameras) and reconstructed in real-time through the optical motion capture software Motive. Flat and flexible 6 mm diameter retroflective markers were used to avoid interfering with the packaging process of the structure. Additional markers were placed on the deployment mechanism roller mounts and on the hinges at their base to characterize the deployment of the mechanism's rollers.

To describe the deployment of the DOLCE structure, two metrics of interest were chosen: the distance of the ends of the strips from the central axis of the deployment mechanism (R in Figure 11), and the envelope of heights of the center of the strips (H_{max} and H_{min} in Figure 11). R describes the deployed size of the structure over time and H_{max} and H_{min} define the keep-out volume around the deployable structure to avoid interference with other payloads.

Images captured during and post deployment are shown in Figure 10c and Figure 10d, respectively. The results for a typical experiment are reported in Figure 12. Figure 12a shows that the four corners of the structure deploy radially from the center in a synchronized fashion and reach their fully deployed configuration after approximately 690 ms. The distance of each corner from the center deviates less than 2% from the mean distance at all times. The plot in Figure 12b shows the trajectories of the points located at the center of each strip, where the height of the deployable structure reached its extreme values. The reference height $z = 0$ corresponds to the nominal height of the structure at the end of deployment, set by the location of the cord attachment point to the center of the mechanism. This plot suggests that the deployment requires a total height of about 550 mm, mostly extending upwards from its initial folded configuration. The four mechanism tensioning roller assemblies were released with a mean delay of 29 ms from each other, and a maximum delay of 90 ms between the release of the first and last roller.

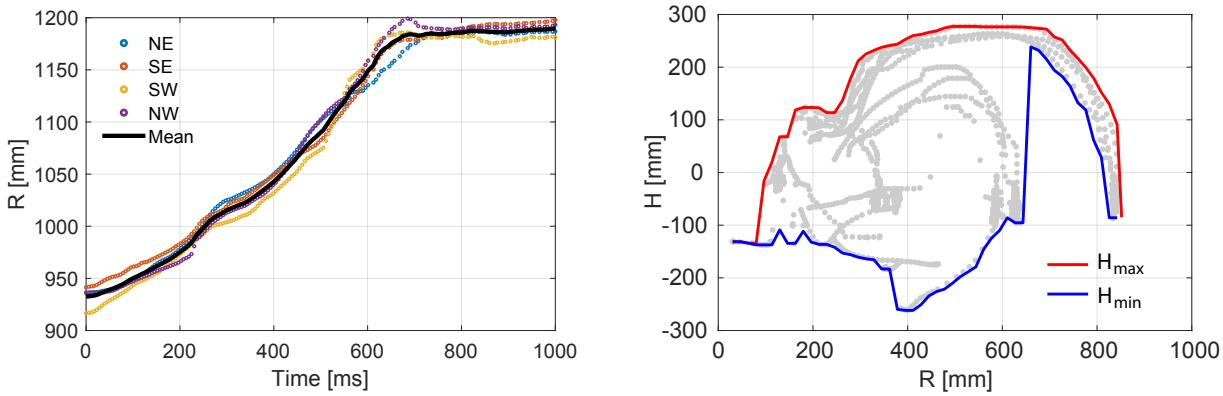

(a) Distance of corners of the structure from central axis.

(b) Envelope of center strip heights.

Fig. 12 Experimental results from deployment tests.

IV. Engineering Model Testing

Three types of tests have been conducted on the DOLCE EM to-date: (i) integrated system functional tests; (ii) launch load tests; and (iii) accelerated aging tests. Thermal vacuum tests have been performed at the component level and will be performed on the DOLCE FM and will not be discussed further here.

A. Integrated Functional Tests

The DOLCE EM functional tests were performed at the Caltech Space Structures Clean Room in Pasadena and consisted of executing all deployments in the same sequence as on orbit. The integrated DOLCE EM used in these tests is shown in Figure 13a. Flight-like components were used with the exception of cables and harnessing, some cable management features, a few simple brackets, and lubricants.

The first deployment steps result in full deployment of the camera boom and partial deployment of the diagonal booms, as shown in Figure 13b. Once the cameras had been deployed, they were used to successfully image the subsequent deployment steps. The diagonal booms are only partially deployed at this stage as the length of the cord that they deploy is limited by a spring retractor. In the next step, the deployable structure is uncoiled by the mechanism into the star shape shown in Figure 13c. The uncoiling of the structure releases additional cord, so the diagonal booms can extend to their fully deployed position as shown in Figure 13d. Finally, four release actuators in the mechanism are energized, releasing the four arms that maintain the deployable structure in the star shape, and hence the structure fully deploys as shown in Figure 13e.

In total, three integrated DOLCE EM functional tests have been performed to-date. The first two tests revealed two design issues that resulted in incomplete deployment. The first issue was caused by torsional twisting of the diagonal booms during the structure's deployment. This issue was not observed during the deployment tests in the motion capture laboratory as the aluminum extrusions used as surrogates for the diagonal booms were significantly stiffer than the booms and did not twist. The issue was resolved by connecting the booms to slightly slack wires that limit the amount a boom can twist to a few degrees, based on the slack in the wire. The second issue was that the deployed position of the mechanism's releasable arms was high enough for the structure to get caught in some sharp features during its deployment. The hypothesis about why this issue was not observed during the previous deployment tests is that a feature locking the releasable arms in place had not been implemented yet, resulting in bouncing of these arms after deployment. Our hypothesis is that this bouncing resulted in the structure getting released after it was initially caught in the same sharp features. We resolved this issue by both smoothing the sharp features as well as slightly shifting the location of some components to increase their distance from the structure during its deployment. The third integrated functional test demonstrated the resolution of these design issues and resulted in complete deployment.

Fig. 13 (a) Integrated DOLCE EM in fully stowed configuration; (b) after complete camera boom deployment and diagonal boom partial deployment; (c) structure uncoiled into the star shape; (d) diagonal boom complete deployment; and (e) after structure complete deployment.

B. Launch Load Tests

Launch load testing was conducted on the integrated DOLCE EM at Experior Laboratories in Oxnard, California. The unit used in these tests (shown in Figure 14a) was the same as the one in the functional tests. Three of the four diagonal booms and the camera boom assembly were replaced with mass models to prevent a potential over-test of these units as they will be included in the final acceptance testing prior to launch. The test sequence is shown in Figure 14b. The tests and MPE levels were specified by Momentus Space and test parameters were derived from the MPE for protoflight-level testing (Table 6).

Table 6 DOLCE EM Launch Load Test Levels

Test	MPE	Test Parameters
Sine Sweep	N/A	20-2000 Hz, 2 Oct/min, 0.5 g
Sine Burst	12.9 g laterally	16.125 g laterally, 15 cycles at 15 Hz
	7.4 g axially	9.25 g axially, 15 cycles at 15 Hz
Random Vibration	8.3 g_{RMS}	12.3 g_{RMS}, 1 minute
	100 Hz: 40 g	100 Hz: 57 g
Shock	410 Hz: 250 g	410 Hz: 355 g
	1000 Hz: 250 g	1000 Hz: 355 g

The DOLCE fundamental frequency in the lateral directions was measured to be 72 Hz in one axis and 69 Hz in the other. The radial asymmetry of the imaging subsystem located at the top of the payload accounts for this difference in the otherwise radially symmetric structure. In the axial direction, peaks in the frequency response were observed at 112 Hz and 330 Hz. Two design issues were discovered during the random vibration test: (i) rotation of the mechanism's central stage and (ii) unintended separation of the release actuators locking the tensioning roller assemblies. Both issues were temporarily resolved by mechanical restraints, the random vibration test was restarted, and the test sequence continued. After the conclusion of each test, the unit was visually inspected and a sine sweep was performed to compare the frequency response before and after the test. No visual damage and no meaningful changes in the frequency response were observed. After the launch load test sequence was completed, DOLCE was successfully deployed at Caltech.

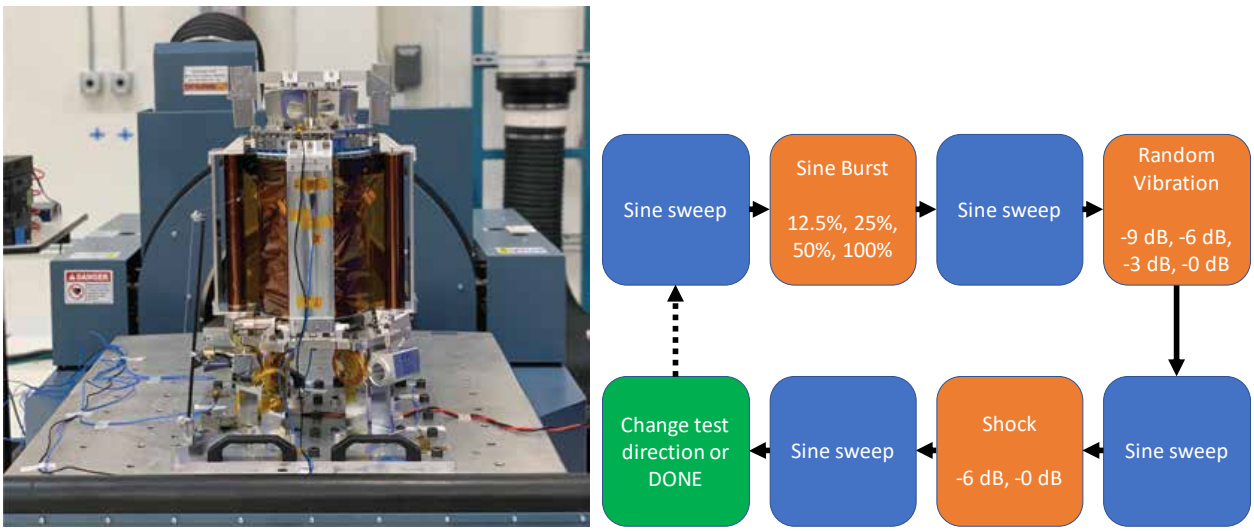

(a) (b)

Fig. 14 (a) DOLCE EM on shaker table at Experior Laboratories; (b) launch load test flow chart conducted on DOLCE EM.

During design, the high gear ratio of the central stage's worm gear was assumed to be sufficient to prevent unintended

rotation and therefore no brake was specified for its motor. To mitigate this issue the same passive brake included in the roller motors will be included in the central stage motor. The unintended separation of the release devices was only observed in the actuators oriented in the direction of the test. Two mitigation strategies are currently being evaluated: (i) re-orientation of the release devices so that they are removed from the load-path and (ii) replacement of the release devices with a high-strength unit.

C. Accelerated Aging Tests

To evaluate the effects of long-term stowage on the DOLCE deployable structure, we subjected the DOLCE structure in the mechanism to simulated accelerated aging by means of elevated temperature and afterwards we performed a deployment test.

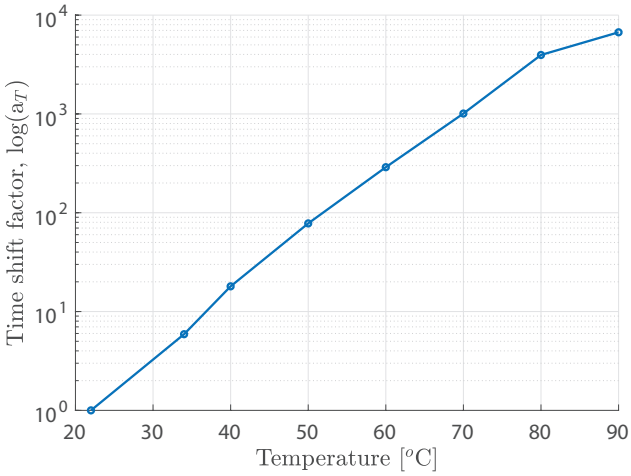

(a)

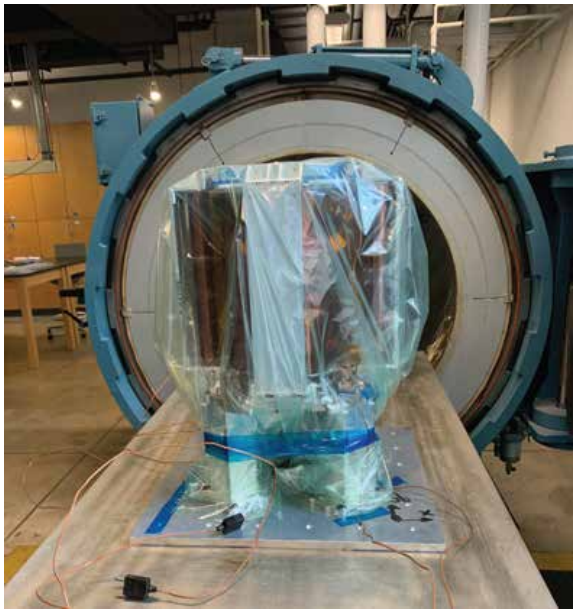

(b)

Fig. 15 (a) Experimentally obtained time-shift factors for longeron laminate; (b) DOLCE EM being placed for 24 hours at 60 °C, simulating 9 months of aging.

The viscoelastic properties of polymers are known to have time (t) and temperature (T) dependency. The time-dependent behavior tests are accelerated by combining time-temperature effects through a correction known as the time-shift factor a_T in the real time-scale t. The reduced time t' is related to the real time by

$$t' = \int_0^t \frac{\mathrm{d}\tau}{a_T(T)} \tag{4}$$

We used an experimental approach to calculate the time-shift factor for the longeron laminate with cyanate ester resin. A bending relaxation test was carried out by imposing a curvature in the test samples using the platen test setup [27]. The test samples were 70 mm long by 20 mm wide [±45 PWGF /0 UDCF/±45 PWGF][±45 PWGF][±45 PWGF /0 UDCF/±45 PWGF] laminates corresponding to the web-section of the DOLCE structure's longerons. After autoclave curing, the test samples were sprayed with white and black speckles for DIC measurements. Bending relaxation tests were carried out at temperatures ranging from 22 °C to 90 °C. At each temperature, the sample was mounted between the platens and the temperature of the chamber was set to the desired value. The temperature inside the thermal chamber was measured using two thermocouples throughout the experiment. Until the temperature reached equilibrium, the thermal expansion of the setup was compensated by manually adjusting the extension to maintain the load reading at approximately zero. In each test, a curvature of 0.05 mm^{-1} was imposed and held for 3 hours. The time-varying force measurement was recorded from the load cell. The actual curvature (κ) and the lever arm (y) were measured using DIC.

The relaxation modulus, $D(t)$ was calculated from

$$D(t) = \frac{F(t) \times y}{\kappa} \tag{5}$$

Once the relaxation modulus at each temperature had been obtained, it was shifted to the reference temperature $T_0 = 22$ °C to obtain the master curve. The time-shift factors (shown in Figure 15a) were determined such that the shifted relaxation modulus curves form a single smooth curve. Based on the results from Figure 15a the DOLCE EM mechanism and structure assembly was wrapped in a vacuum bag to prevent contamination and placed in an autoclave (Figure 15b) at 60 °C and atmospheric pressure for 24 hours, corresponding to approximately 9 months at 22 °C. After removing the assembly from the autoclave, the structure was uncoiled and deployed. No noticeable difference in deployment behavior was observed.

V. Conclusion

The transition of the ultralight Caltech SSPP structure and deployment mechanism from lab prototypes to integrated and tested engineering models for the DOLCE technology demonstration payload has been demonstrated. Deployment testing at the mechanism-structure level and the integrated DOLCE level, launch load analysis and testing, and accelerated aging testing have been conducted and the SSPD-1 mission is on track for the first on-orbit demonstration of the key space-based solar power enabling technologies proposed by Caltech six years ago. The structure on DOLCE measures 1.7 m × 1.7 m and weighs 99 g/m^2. In future milestones, the Caltech SSPP structure will be scaled to larger sizes demonstrating even lower areal densities, and will be integrated with photovoltaics and electronically steerable power-beaming antennas.

Acknowledgments

Financial support from the Space Solar Power Project at Caltech is gratefully acknowledged.

References

[1] Glaser, P. E., "Power from the sun: Its future," *Science*, Vol. 162, No. 3856, 1968, pp. 857–861.

[2] Mankins, J. C., "A technical overview of the "Suntower" solar power satellite concept," *Acta Astronautica*, Vol. 50, No. 6, 2002, pp. 369–377.

[3] Mankins, J., "SPS-ALPHA: The First Practical Solar Power Satellite via Arbitrarily Large Phased Array," Tech. rep., Artemis Innovation Management Solutions LLC, 2012.

[4] Mankins, J., *The case for space solar power*, Virginia Edition Publishing, 2014.

[5] Oda, M., "Realization of the Solar Power Satellite Using the Formation Flying Solar Reflector," *NASA Formation Flying symposium, Washington DC, Sept. 14-16, 2004*, 2004. URL `http://ci.nii.ac.jp/naid/10019656944/en/`.

[6] Seboldt, W., Klimke, M., Leipold, M., and Hanowski, N., "European sail tower SPS concept," *Acta Astronautica*, Vol. 48, No. 5, 2001, pp. 785–792.

[7] Sasaki, S., Tanaka, K., Higuchi, K., Okuizumi, N., Kawasaki, S., Shinohara, N., Senda, K., and Ishimura, K., "A new concept of solar power satellite: Tethered-SPS," *Acta Astronautica*, Vol. 60, No. 3, 2007, pp. 153–165.

[8] Jaffe, P., Borders, K., Browne, C., DePuma, C., Longbottom, L., Nisar, H., Simlot, V., Bar-Cohen, A., McSpadden, J., Brandt, R., Conrad, E., Duncan, K., Rowley, W., Thampan, T., Garretson, P., Mankins, J. C., Potter, S., Sundberg, E., and Walts, A., "Opportunities and Challenges for Space Solar for Remote Installations," , 2019. Technical Report AD1082903.

[9] Arya, M., Lee, N., and Pellegrino, S., "Ultralight structures for space solar power satellites," *3rd AIAA Spacecraft Structures Conference*, 2016, p. 1950.

[10] Kelzenberg, M. D., Espinet-Gonzalez, P., Vaidya, N., Roy, T. A., Warmann, E. C., Naqavi, A., Loke, S. P., Huang, J.-S., Vinogradova, T. G., Messer, A. J., Leclerc, C., Gdoutos, E. E., Royer, F., Hajimiri, A., Pellegrino, S., and Atwater, H. A., "Design and Prototyping Efforts for the Space Solar Power Initiative," *IEEE PVSC*, 2017.

[11] Gdoutos, E. E., Leclerc, C., Royer, F., Kelzenberg, M. D., Warmann, C., Emily, Espinet-Gonzalez, P., Vaidya, N., Bohn, F., Abiri, B., Hashemi, M. R., Gal-Katziri, M., Fikes, A., Atwater, H. A., Hajimiri, A., and Pellegrino, S., "A lightweight tile structure integrating photovoltaic conversion and RF power transfer for space solar power applications," *AIAA SciTech Forum*, 2018.

[12] Hashemi, M. R. M., Fikes, A. C., Gal-Katziri, M., Abiri, B., Bohn, F., Safaripour, A., Kelzenberg, M. D., Warmann, E. L., Espinet, P., Vaidya, N., Gdoutos, E. E., Leclerc, C., Royer, F., Pellegrino, S., Atwater, H. A., and Hajimiri, A., "A flexible phased array system with low areal mass density," *Nature Electronics*, Vol. 2, No. 5, 2019, pp. 195–205. doi:10.1038/s41928-019-0247-9, URL https://doi.org/10.1038/s41928-019-0247-9.

[13] Gdoutos, E., Leclerc, C., Royer, F., Türk, D. A., and Pellegrino, S., "Ultralight Spacecraft Structure Prototype," *AIAA SciTech Forum*, 2019. doi:10.2514/6.2019-1749, URL https://arc.aiaa.org/doi/abs/10.2514/6.2019-1749.

[14] Pedivellano, A., Gdoutos, E. E., and Pellegrino, S., "Sequentially controlled dynamic deployment of ultra-thin shell structures," *AIAA SciTech Forum*, 2020.

[15] Gdoutos, E., Truong, A., Pedivellano, A., Royer, F., and Pellegrino, S., "Ultralight Deployable Space Structure Prototype," *AIAA Scitech 2020 Forum*, 2020. doi:10.2514/6.2020-0692, URL https://arc.aiaa.org/doi/abs/10.2514/6.2020-0692.

[16] Pellegrino, S., Atwater, H., Hajimiri, S. A., Gdoutos, E. E., Leclerc, C., Royer, F. A., and Pedivellano, A., "Coilable Thin-Walled Longerons and Coilable Structures Implementing Longerons and Methods for Their Manufacture and Coiling," , 2018. US Patent 20200024007A1, pending.

[17] Pellegrino, S., Gdoutos, E. E., and Pedivellano, A., "Actively Controlled Spacecraft Deployment Mechanism," , 2018. US Patent 20200130868A1, pending.

[18] Murphey, T. W., and Banik, J., "Triangular rollable and collapsible boom," , Mar. 1 2011. US Patent 7,895,795.

[19] Leclerc, C., Wilson, L. L., Bessa, M. A., and Pellegrino, S., "Characterization of ultra-thin composite triangular rollable and collapsible booms," *4th AIAA Spacecraft Structures Conference*, 2017, p. 0172.

[20] Leclerc, C., and Pellegrino, S., "Reducing Stress Concentration in the Transition Region of Coilable Ultra-Thin-Shell Booms," *AIAA SciTech Forum*, 2019. doi:10.2514/6.2019-1522, URL https://arc.aiaa.org/doi/abs/10.2514/6.2019-1522.

[21] Royer, F., and Pellegrino, S., *Buckling of Ultralight Ladder-type Coilable Space Structures*, 2020.

[22] Brinkmeyer, A., Pellegrino, S., and Weaver, P. M., "Effects of long-term stowage on the deployment of bistable tape springs," *Journal of Applied Mechanics*, Vol. 83, No. 1, 2016, p. 011008.

[23] Medina, K., Rose, T., and Francis, W., "Long-term Stress Rupture Limitations of Unidirectionasl High Strain Composites in Bending," *Proceedings of the American Society for Composites—Thirty-third Technical Conference*, 2018.

[24] Ubamanyu, K., Ghedalia, D., Hasanyan, A. D., and Pellegrino, S., "Experimental Study of Time-dependent Failure of High Strain Composites," *AIAA Scitech 2020 Forum*, 2020, p. 0207.

[25] Grygorczuk, J., Wisniewski, Ł., Kedziora, B., Borys, M., Przybyła, R., Kucinski, T., Ossowski, M., Konior, W., Krömer, O., Spohn, T., et al., "Hammering mechanism for hp3 experiment (insight)," *Proceedings of the 43rd Aerospace Mechanisms Symposium*, NASA Ames Research Center, 2016, pp. 415–428.

[26] LoSchiavo, M., Phillips, R., Mikhaylov, R., and Braunschweig, L., "from Commercial-Off-the-Shelf to Flight-Qualified Motors, Gearboxes, and Detent Brakes: Overcoming Issues and Lessons Learned," ????

[27] Yee, J., and Pellegrino, S., "Biaxial bending failure locus for woven-thin-ply carbon fibre reinforced plastic structures," *46th AIAA/ASME/ASCE/AHS/ASC Structures, Structural Dynamics and Materials Conference*, 2005, p. 1811.